Quantitative Research on Cracks in Pipe Based on Magnetic Field Response Method of Eddy Current Testing

Feng Jiang [1,2], Shulin Liu [2], and Li Tao [3]

[1] School of Electrical and Information Engineering
Changzhou Institute of Technology, Changzhou, 213032, China
jiangf@jsit.edu.cn

[2] School of Mechatronics Engineering and Automation
Shanghai University, Shanghai, 200072, China
lsl346@shu.edu.cn

[3] Library and Information Center
Jiangsu Vocational College of Information Technology, Wuxi, 214153, China
tao_li_@126.com

Abstract ─ The quantitative evaluation of defects in eddy current testing is of great significance. Impedance analysis, as a traditional method, is adopted to determine defects in the conductor, however, it is not able to depict the shape, size and location of defects quantitatively. In order to obtain more obvious characteristic quantities and improve the ability of eddy current testing to detect defects, the study of cracks in metal pipes is carried out by utilizing the analysis method of three-dimensional magnetic field in present paper. The magnetic field components in the space near the crack are calculated numerically by using finite element analysis. The simulation results confirm that the monitoring of the crack change can be achieved by measuring the magnetic field at the arrangement positions. Besides, the quantitative relationships between the shape, length of the crack and the magnetic field components around the metal pipe are obtained. The results show that the axial and radial magnetic induction intensities are affected more significantly by the cross-section area of the crack. B_z demonstrates obvious advantages in analyzing quantitatively crack circumference length. Therefore, the response signal in the three-dimensional direction of the magnetic field gets to intuitively reflect the change of the defect parameter, which proves the effectiveness and practicability of this method.

Index Terms ─ Cracks evaluation, Eddy current testing, finite element method, magnetic field, pipe.

I. INTRODUCTION

Electromagnetic nondestructive testing is a kind of testing method to evaluate the structure and related properties of tested materials by utilizing the changes of electromagnetic characteristics under the action of the electromagnetic field [1-3]. It mainly includes eddy current testing (ECT), magnetic particle testing (MT) and magnetic flux leakage (MFL) testing. With the development of technology, a great many new electromagnetic nondestructive testing methods have appeared, such as alternating current field measurement (ACFM) and metal magnetic memory (MMM) testing. ECT, MFL and ACFM are commonly used to detect defects, although they differ in their principles of measurement.

Among the three methods mentioned above, what has been used in ECT as the physical quantity is coil impedance [4-6], while the physical quantity measured by MFL and ACFM is magnetic field which is a three-dimensional physical quantity that adequately characterizes geometric parameters such as length, as well as width of a defect. Therefore, the latter two methods gain significant advantages over ECT from the perspective of defect information contained in physical quantities. On the other hand, what also have been compared are excitation modes of three electromagnetic nondestructive testing. The excitation source is used in the local magnetization of the workpiece by MFL [7-9]. And DC magnetization has a high requirement for the current source. The excitation current is generally shown from several amperes to hundreds of amperes, and the electrical equipment is relatively complicated. Moreover, the direction of defects has exerted a great influence on the magnetic leakage field. Similarly, the excitation coil of ACFM needs to induce parallel and approximately uniform currents on the specimen surface, so as to generate approximately uniform alternating electromagnetic field [10-12]. Undoubtedly, the uniform

Submitted On: August 5, 2019
Accepted On: February 23, 2020

https://doi.org/10.47037/2020.ACES.J.360114

eddy current requires higher requirements on the structure of excitation devices. In addition, when the current direction is parallel to that of the crack, the sensitivity of the detection explores the lowest level and the missed detection may occur. However, the induced eddy current generated by the excitation coil of ECT is in the circumferential direction. Defects in any direction will cause a change in the eddy current, thereby generating a disturbing eddy current field. Moreover, the excitation method used in ECT is simple, convenient and easy under operation. Therefore, compared with the other two methods, the traditional ECT exhibits certain strengths according to the analysis of the excitation modes.

Considering the advantages and disadvantages of the above testing methods, the configurations of traditional ECT are retained, and the magnetic field analysis of MFL and ACFM is adopted in the present paper, so as to implement the quantitative study of the shape and circumference length of cracks in metal pipelines.

II. MATHEMATICAL MODEL OF THREE-DIMENSIONAL EDDY CURRENT FIELD

A typical solution domain V of the eddy current problem is assumed, where V_1 is the eddy current zone containing the conductive medium without the source current and V_2 is the non-eddy current zone including the given source current. S_{12} is the internal interface of V_1 and V_2. The outer boundary S of solution domain V is divided into S_B and S_H. The normal component of the magnetic induction intensity is given on S_B, and S_H provides the tangential component of the magnetic induction intensity.

Maxwell's equations describe the macroscopic properties of the electromagnetic field, which is not always convenient to be solved directly. ***A***, ***Φ-A*** method will be used to establish the mathematical model of eddy current analysis. In the eddy current area, magnetic vector potential $\boldsymbol{A}$ and scalar potential Φ are used as unknown functions, and in the non-eddy current area, only $\boldsymbol{A}$ is used as unknown functions. Substituting $\boldsymbol{B} = \nabla \times \boldsymbol{A}$ and $\boldsymbol{E} = -\frac{\partial \boldsymbol{A}}{\partial t} - \nabla\phi$ into Maxwell's equations, and specifying $\nabla \cdot \boldsymbol{A} = 0$, the governing equations and boundary conditions of eddy current field in region V are illustrated as follows:

$$\left.\begin{aligned} &\nabla \times \left(\nu \nabla \times \boldsymbol{A}\right) - \nabla\left(\nu \nabla \cdot \boldsymbol{A}\right) + \sigma \frac{\partial \boldsymbol{A}}{\partial t} + \sigma \nabla \phi = 0 \quad \text{(a)} \\ &\nabla \cdot \left(-\sigma \frac{\partial \boldsymbol{A}}{\partial t} - \sigma \nabla \phi\right) = 0 \quad \text{(b)} \end{aligned}\right\} \text{ in the } V_1, \tag{1}$$

$$\nabla \times \left(\nu \nabla \times \boldsymbol{A}\right) - \nabla\left(\nu \nabla \cdot \boldsymbol{A}\right) = \boldsymbol{J}_s \quad \text{in the } V_2, \tag{2}$$

$$\left.\begin{aligned} &\boldsymbol{n} \times \boldsymbol{A} = 0 \quad \text{(a)} \\ &\nu \nabla \cdot \boldsymbol{A} = 0 \quad \text{(b)} \end{aligned}\right\} \text{ on the } S_B, \tag{3}$$

$$\left.\begin{aligned} &\boldsymbol{n} \cdot \boldsymbol{A} = 0 \quad \text{(a)} \\ &\left(\nu \nabla \times \boldsymbol{A}\right) \times \boldsymbol{n} = 0 \quad \text{(b)} \end{aligned}\right\} \text{ on the } S_H, \tag{4}$$

$$\left.\begin{aligned} &\boldsymbol{A}_1 = \boldsymbol{A}_2 \quad \text{(a)} \\ &\nu_1 \nabla \cdot \boldsymbol{A}_1 = \nu_2 \nabla \cdot \boldsymbol{A}_2 \quad \text{(b)} \\ &\nu_1 \nabla \times \boldsymbol{A}_1 \times \boldsymbol{n}_{12} = \nu_2 \nabla \times \boldsymbol{A}_2 \times \boldsymbol{n}_{12} \quad \text{(c)} \\ &\boldsymbol{n} \cdot \left(-\sigma \frac{\partial \boldsymbol{A}}{\partial t} - \sigma \nabla \phi\right) = 0 \quad \text{(d)} \end{aligned}\right\} \text{ on the } S_{12}, \tag{5}$$

where σ is the electric conductivity, ν is the magnetoresistance, J_s is the source current density, n is the unit normal vector of S, n_{12} is the unit normal vector of S_{12}, and the direction is from V_1 to V_2.

However, the analytical method or the field-to-circuit method is unable to deal with a large number of engineering problems involving complex geometric and physical parameters [13-15]. Thanks to the rapid development of computer technology, it has promoted the progress of numerical analysis methods. Most importantly, the finite element method is the most widely used numerical method at present. Compared with other numerical methods, the finite element method shows prominent characteristics [16-18]. The finite element mesh can easily simulate the boundary and interface of different shapes. The discrete equations attained by the finite element method display sparse symmetric coefficient matrix, which simplifies the solution to the equations, and reduces the computer storage and computing time correspondingly.

Next, COMSOL Multiphysics, as the finite element analysis software is utilized to model the metal pipe and defects. Based on the three-dimensional magnetic field analysis, the solution in the specified field is obtained by the finite element method.

III. QUANTITATIVE STUDY OF CRACKS IN PIPES

A. Section shape of cracks

Figure 1 presents the three-dimensional model with a circumferential crack on the inner surface of the metal pipe. The cross-section shapes of the cracks are rectangle, semicircle and triangle, and their openings are kept at 4 mm and their depths are 2 mm. Only the influence of section shapes is considered here, so the three kinds of cracks are all-circle ones in the plane perpendicular to the axis. In addition, the excitation coil is a cylindrical coil coaxial with the metal pipe. The geometric parameters of the coil are listed as follows: inner radius r_{c1} = 8 mm, outer radius r_{c2} = 12 mm and height h = 6 mm. Based on such considerations, the three-dimensional model can be simplified into a two-dimensional axisymmetric one. In

this way, the finite element model gets to be simplified, and a more refined mesh is thus able to be used to improve the computational efficiency. The parameters of the finite element model are set as follows. It is assumed that the surrounding air medium is a cylinder with a radius of 20 mm and a height of 60 mm. Constraint conditions should be applied to the outer boundary and symmetry axis of the model. The central axis of the metal pipe should be set as the axisymmetric condition. The magnetic vector potential of the upper and lower ends of the metal pipe should be zero, and the magnetic insulation condition is applied to the outermost boundary of the air domain. The ultra-fine mesh processing is used, and the mesh is divided using triangular elements. The MUMPS direct solver is used and the relative tolerance is set to 0.001.

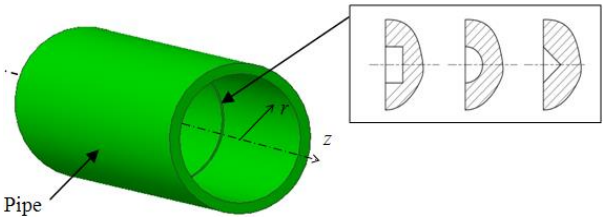

Fig. 1. The three-dimensional schematic diagram of the model.

The radial measurement points are 12.5 mm and 13.5 mm, respectively, and the measurement range in the z direction is from -20 mm to 20 mm. Figure 2 displays the distribution curves of radial and axial magnetic induction intensity under three kinds of cracks with different cross-section shapes. The curves indicated by the circle are the radial and axial magnetic induction intensity at the position of r = 13.5 mm without crack. The magnetic induction intensity varies with the axial distance as shown in Fig. 2, where the location of the excitation coil does not change. During the detection process, the magnetic sensor scans along the axial direction to obtain the magnitude of the magnetic induction intensity at each position.

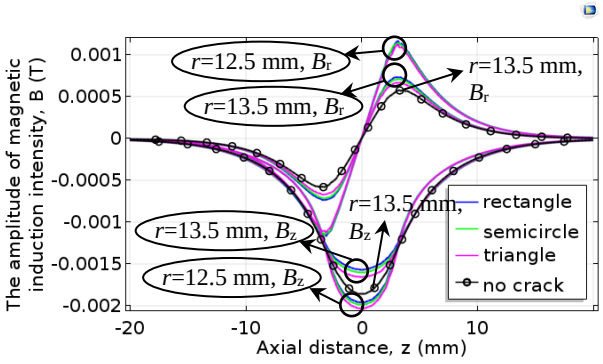

Fig. 2. The distribution curves of radial and axial magnetic induction intensity for cracks with different shapes.

The following four conclusions can be drawn from Fig. 2:

(1) The B_r curves show odd symmetrical distributions, reaching the maximum value at a certain distance in the axial direction. The B_z curves are distributed even symmetrically, with the maximum value at z = 0. As the axial distance increases, the value decreases gradually.

(2) Although the shapes of crack show no influence to the overall distribution of the magnetic induction intensity, it has a certain influence on the values of radial and axial magnetic induction intensity. As can be seen from Fig. 2, regardless of r = 12.5 mm and 13.5 mm, the changes of radial and axial magnetic induction intensities caused by rectangular crack are the most prominent, followed by the semi-circular section. What's more, the triangular section shows the least obvious influence. So, the following conclusion gets to be drawn: the larger the crack section area is, the more obvious the influence on the external magnetic field becomes. It is also helpful for us to judge and analyze the specific shape of crack by means of the change of the external magnetic field.

(3) The above conclusion is further confirmed by the distribution of electromagnetic fields. Figure 3 shows the induced current density inside the pipe and the distribution of contour lines of B_r and B_z near the crack. With the increase of the crack section area, the degree of the influence of the crack on the contour line B_r becomes more obvious. As shown in the black circled part of Fig. 3, it can be clearly seen that the curve near the crack is attracted to the side of the pipe. At this time, the value of the magnetic induction intensity in the vicinity increases. Similarly, as the section area of the crack increases, the degree of the influence of the crack on the contour line B_z becomes more obvious. As shown in the black rectangle marked in Fig. 3, it can be seen that the contour near the crack appears to be free from the restraint of the metal pipe and gradually moves toward the side of the excitation coil. At this time, the magnetic induction intensity near the crack decreases. Therefore, the radial and axial magnetic inductions show the changes shown in Fig. 2. Meanwhile, the electromagnetic field distribution further proves that the radial and axial magnetic induction intensities have opposite changes due to the crack shape.

(4) The following conclusion can be drawn from the results obtained from different radial measurements. On the one hand, the closer to the inner surface of the metal pipe is, the smaller the radial and axial magnetic induction intensities become, which is related to the fact that the external magnetic field is dominated by the source field generated by the coil. On the other hand, the closer to the inner surface

of the metal pipe is, the more obvious the change of magnetic field caused by crack shape can be detected. This characteristic is related to the eddy current field. Cracks with different cross-sections are supposed to cause different eddy currents to be induced on the surface of the metal pipe. And this eddy current will simultaneously induce different electromagnetic fields on the surface of the metal pipe.

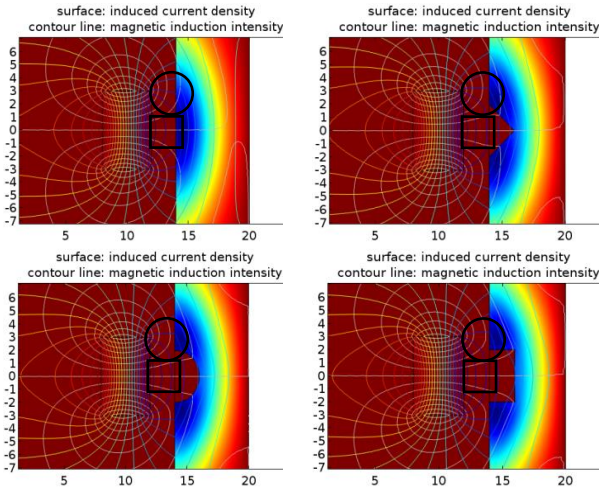

Fig. 3. Distribution of induced current density and magnetic induction intensity contours for cracks with different shapes.

Figure 4 shows the variations in the peak of radial and axial magnetic induction intensity with the cross-sectional area of the crack. As can be seen from Fig. 4, the peak of radial magnetic induction intensity increases with the crack-sectional area and shows a linear relationship. As the cross-sectional area increases from 5 mm^2 to 8 mm^2, the peak value of radial magnetic induction intensity increases by 6.764×10^{-5} T. Similarly, the peak of axial magnetic induction intensity decreases with the cross-sectional area of the crack, and shows a linear relationship. As the cross-sectional area increases from 5 mm^2 to 8 mm^2, the peak value of axial magnetic induction intensity decreases by 8.711×10^{-5} T. The results show that the relationship between the magnetic induction intensity and the cross-sectional area of the crack is linear, which is beneficial to the quantitative identification of the crack shape. In addition, both radial and axial magnetic induction intensity near the pipe can be used for the quantitative analysis of the crack shape, and axial magnetic induction intensity changes more significantly. Through the monitoring and comparison of the magnetic field in two directions, the measurement results can be further confirmed to avoid the influence of external interference. Moreover, effective signals in both directions provide more options for actual detection.

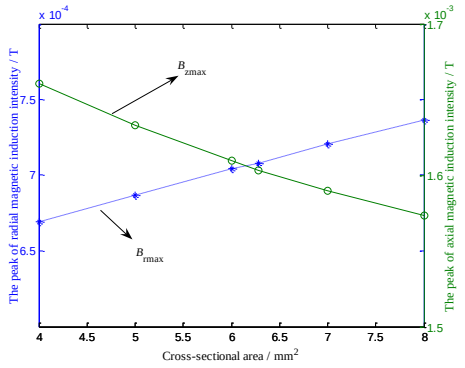

Fig. 4. The relationship between the peak of the magnetic induction intensity and cross-sectional area of the crack.

As the crack shape changes from a rectangle to semicircle and then to triangle, the peak values of axial magnetic induction increase by 2.979×10^{-5} T and 5.732×10^{-5} T, respectively. The change of response is measurable in practice as a result of advances in sensors and signal processing technology. Magnetic sensors based on TMR effects have the virtue of high accuracy, wide linear ranges and strong anti-interference capability, which have been widely used in electromagnetic nondestructive testing. The commercially available TMR2905 sensor, for example, has a sensitivity of 60 mV/V/Oe, noise <5nT/rtHz (@1Hz), and a resolution of 0.01μT. The magnetic sensor is able to completely meet the measurement requirements according to the changes of radial or axial magnetic induction intensities caused by crack shapes. Another noticeable external disturbance is the space geomagnetic field. The magnetic induction intensity of the earth's surface is about 0.5×10^{-4} T. Compared with the changes of the magnetic field caused by crack shapes, this value is still relatively obvious. Thus, some technical means must be adopted to suppress its effect. For instance, the frequency of excitation current is 1 kH_Z, so phase-locked amplifier can be used in the actual detection to remove the signal of non-selected frequency (i.e., noise) and retain the information of selected frequency.

B. Circumferential length of cracks

Six model components with different crack lengths are established in COMSOL Multiphysics. Different from the construction of rectangular or semicircle crack model, the research on the circumference length of crack requires the establishment of three-dimensional model. Compared with the two-dimensional model, the three-dimensional model takes a longer time to calculate. Therefore, the mesh type is adjusted to a free tetrahedral mesh during mesh generation, and its size is defined as refinement. However, it is found that the refined results are obviously not ideal, and the curve generated by post-processing is not smooth, which affects the quantitative

analysis of crack length to some extent. In order to save unnecessary calculation time, the method adopted in this paper is to further refine the key research areas, such as the area near the crack, and select the longest edge to split and the number of refinements to 2. By means of this technique, satisfactory calculation results can be obtained and the calculation time is acceptable. The basic parameters of the metal pipe and coil are exactly the same and the height and depth of the crack section are 2 mm, i.e., the crack section is square. The only difference exists in the circumferential length of the crack. The different lengths in the circumferential direction are represented by the central angles corresponding to the circular arcs, which are 0°, 60°, 120°, 180°, 270° and 360°, respectively, as shown in Fig. 5. Magnetic field measurement positions P1-P4 are selected at 0°, 90°, 180° and 270°, respectively, with radial distance r = 13.5mm. The measurement range of z direction is -20~20mm.

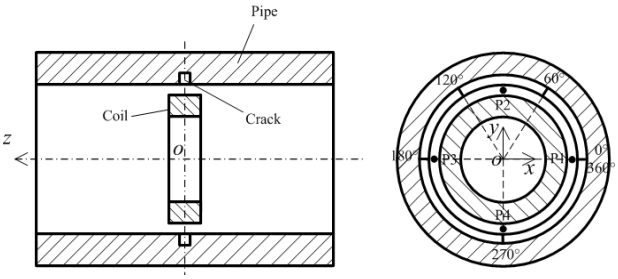

Fig. 5. Model schematic diagram and different length cracks in circumferential direction.

Figure 6 shows the distribution of magnetic induction intensities B_x, B_y and B_z measured at P1-P4 for the metal pipe without crack.

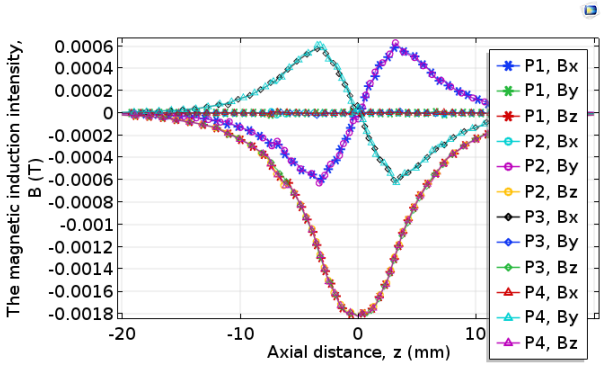

Fig. 6. The magnetic induction intensity at P1-P4 in the absence of cracks.

As shown in Fig. 6, B_x is oddly symmetric with respect to z = 0 at P1. When $z > 0$, B_x is a positive value, and when $z < 0$, B_x becomes negative, while B_y is always zero. Besides, B_z is always negative and even symmetric with respect to z = 0. In order to demonstrate the magnetic induction intensity in the area near P1 more clearly, the three-dimensional magnetic field distributions shown in Fig. 7 are established. As shown in Figs. 7 (a)-(c), the distribution of B_x, B_y and B_z at P1 is completely consistent with the previous two-dimensional figure.

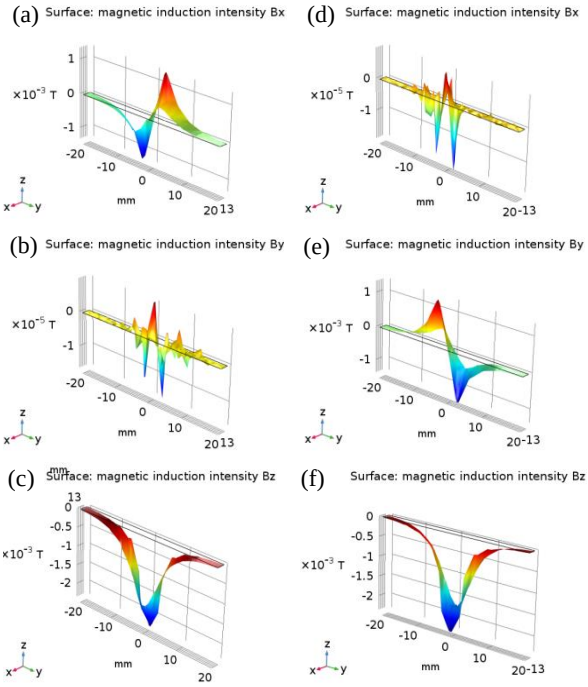

Fig. 7. Three-dimensional distribution of magnetic induction intensity near P1 and P4.

Similarly, the distribution of magnetic fields in three directions at the positions P2-P4 can be obtained from Fig. 6. In order to better understand the distribution of magnetic fields and the relationship, the schematic diagram shown in Table 1 is established.

Table 1: Distributions of magnetic induction intensity at P1-P4

	P1	P2	P3	P4
B_x	Odd symmetry (+)	0	Odd symmetry (-)	0
B_y	0	Odd symmetry (+)	0	Odd symmetry (-)
B_z	Even symmetry	Even symmetry	Even symmetry	Even symmetry

In the table, "+" indicates that the value of the magnetic induction intensity is the same as the symbol of the position value, while "-" suggests that the value

of the magnetic induction intensity is opposite to the symbol of the position value. In addition, the distribution of the magnetic induction intensity near P4 can be understood according to the three-dimensional figures shown in Figs. 7 (d)-(f).

Based on the above analysis, the influence of circumference length of crack on B_x is further analyzed. As shown in Fig. 8 (a), when there is no crack, that is, the corresponding angle of the crack is 0°, B_x at P1 and P3 would be symmetrically distributed. B_x at P2 and P4 are almost zero. As shown in Fig. 8 (b), when a crack with a central angle of 60° appears, the magnetic induction intensity at P1 is expected to increase to some extent, while the B_x of the other three positions are basically unchanged. Under such circumstance, the B_x at P1 and P3 is no longer symmetric. As can be seen from Fig. 8 (c), when the corresponding central angle of the crack increases from 60° to 120°, the magnetic induction intensity at P1 increases slightly, while the magnetic induction intensity at P3 changes a bit. Apart from those, as shown in Fig. 8 (d), when the corresponding central angle of the crack goes up from 120° to 180°, the magnetic induction intensity at P3 increases significantly. Meanwhile, the B_x at P1 and P3 are distributed symmetrically again. However, compared with the symmetry shown in Fig. 8 (a), both of them increase in amplitude. As depicted in Fig. 8 (e), when the corresponding central angle of the crack increases from 180° to 270°, double peaks appear at P4, in addition to a certain increase at P3. What's more, as shown in Fig. 8 (f), when the corresponding central angle of the crack increases from 270° to 360°, double peaks of the magnetic induction intensity observed in Fig. 8 (e) disappear because the model becomes an axisymmetric structure again. B_x at P1 also increases. At this time, the distributions of the magnetic induction intensity at four positions are similar to those without cracks. The difference is that the values of B_x at P1 and P3 increase significantly.

In the light of the previous analysis of changes of B_x, the schematic diagram shown in Table 2 is established, in which "↑" indicates a significant increase in the magnetic induction intensity, and "↗" refers to a certain increase in the magnetic induction intensity, and the symbol "—" suggests few changes appear in the magnetic induction intensity.

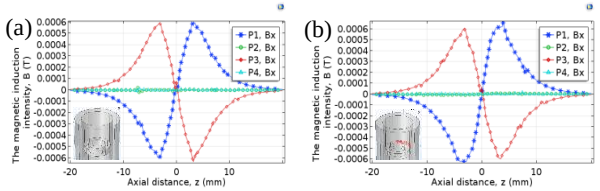

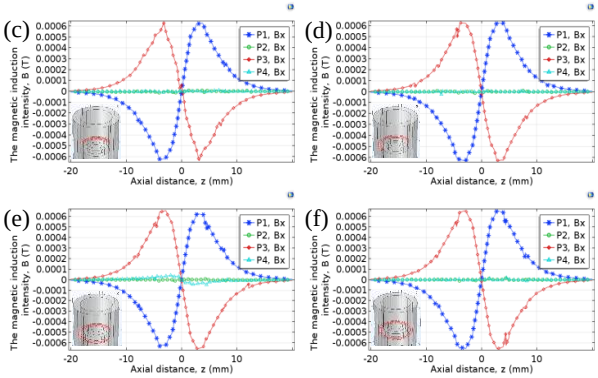

Fig. 8. B_x distribution for different circumferential lengths of cracks.

Table 2: The variation of B_x with the circumference length of crack at P1-P4

	P1	P2	P3	P4
0°	Symmetry with P3 (+)	0	Symmetry with P1 (+)	0
60°	↑	—	—	—
120°	↗	—	↗	—
180°	Symmetry with P3 (+)	—	↑, Symmetry with P1 (+)	—
270°	—	—	↑	Double peak appears
360°	↑, Symmetry with P3 (+)	—	Symmetry with P1 (+)	Double peak disappears

Therefore, the circumference length of crack mainly has a certain influence on B_x at P1 and P3, and exerts little effect on B_x at P2 and P4. By comparing the symmetry of B_x at P1 and P3, the length of the crack in the circumferential direction, thus, gets to be deduced.

Then, the effect of the circumference length on B_y is studied, as shown in Fig. 9. By monitoring the B_y at the P1, it can be found that only in the absence of crack and full-circumferential cracks, does no double peaks occur, and any other circumferential cracks would result in double peak in B_y. Moreover, the amplitude of the peak is not significantly affected by the circumference length of the crack. By monitoring B_y at P3, only when half-circumferential cracks are present and the phenomenon of double peaks appears, will no other circumferential cracks of any length lead to the double peaks in B_y. There is a slight change in B_y at P2 and P4, which, however, is not obvious. Therefore, several other special cracks, such as half-circumferential and whole-circumferential ones, get to be qualitatively assessed by the detection of B_y at P1 and P3.

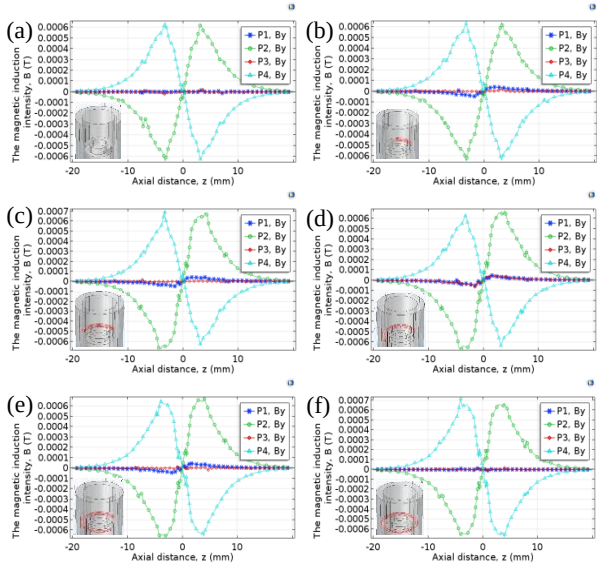

Fig. 9. B_y distribution for different circumferential lengths of cracks.

Finally, what is analyzed hereby is the influence of circumference length on B_z, as shown in Fig. 10. Based on the changes of B_z in Fig. 10, the schematic diagram presented in Table 3 is established. In the table, "↓" indicates a significant decrease in the peak of the magnetic induction intensity, and "↘" reveals a certain decrease in the peak of the magnetic induction intensity. Moreover, "—" shows that the peak of the magnetic induction intensity proves no change. As can be seen from the table, peaks of B_z at P1-P4 decrease sequentially with the ascendance of the circumference length of the crack. Therefore, circumference length of crack can also be quantitatively evaluated by analyzing the change of B_z.

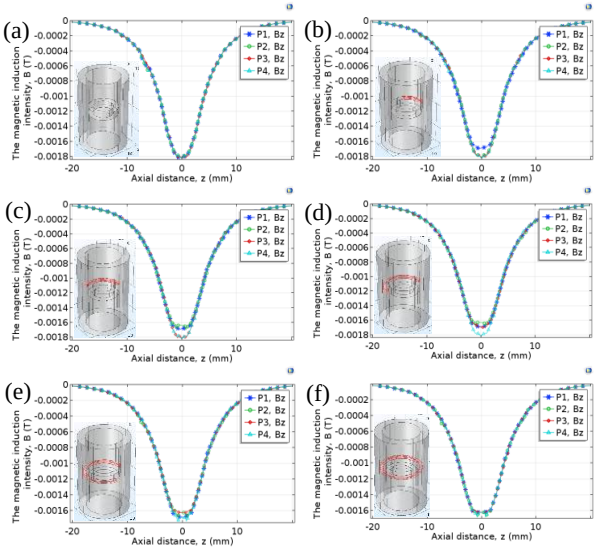

Fig. 10. B_z distribution for different circumferential lengths of cracks.

Table 3: The variation of B_z with the circumference length of crack at P1-P4

	P1	P2	P3	P4
0°	Even symmetry	Even symmetry	Even symmetry	Even symmetry
60°	↓	—	—	—
120°	—	↓	—	—
180°	—	—	↓	—
270°	—	—	—	↓
360°	↘	—	—	↘

Figure 11 shows the relationship between the abrupt positions of the *z*-direction component of the magnetic induction intensity and the different crack lengths. Crack length is represented by the corresponding central angle, and eight types of circumferential cracks with different central angles of 0°, 60°, 120°, 180°, 240°, 270°, 300° and 360° are used. The abrupt position of the *z*-direction component of the magnetic induction intensity is represented by the arc length corresponding to the measured radius of 13.5 mm. As shown in Fig. 11, there is an obvious linear relationship between the circumference length of the crack and the abrupt location of the magnetic induction intensity. In the test, the magnetic sensor is scanned along the circumference of r = 13.5 mm. By monitoring the change of the magnetic field, the information about crack location and crack length can be obtained in time. In addition, the magnetic field is approximately reduced from 1.8×10^{-3} T to 1.6×10^{-3} T for the circumferential cracks studied in this paper, and the abrupt change of about 0.2×10^{-3} T is relatively large, so the detection effect is quite obvious. Thus, it can not only quantitatively analyze the shape of the crack section, but also quantitatively understand the circumference length of the crack by using the characteristics of the magnetic field.

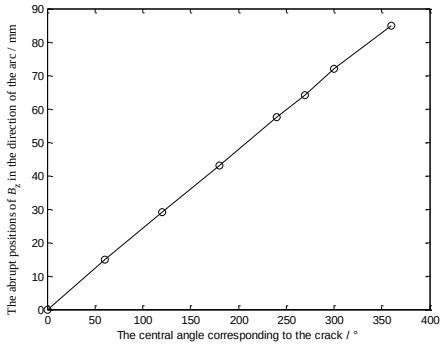

Fig. 11. The relationship between the abrupt position of B_z and the central angle of the crack.

In conclusion, the three directions of the magnetic induction intensity demonstrate their own characteristics in evaluating the circumference length of crack. The B_y is adopted to evaluate several special cracks, but it is not suitable for the quantitative study of crack lengths.

Furthermore, B_z suggests obvious advantages in the quantitative analysis of cracks. Meanwhile, B_x, to some extent, can also meet the demand of the quantitative analysis of circumference lengths in cracks and judge several special lengths.

IV. CONCLUSION

In present paper, the relationship between the crack in metal pipe and the magnetic field in the surrounding space is studied in detail by means of finite element simulation. It can be observed from these analyses that the eddy current field can reflect details such as crack shapes and circumference lengths. These results show that the eddy current testing based on the analysis of the three-dimensional magnetic field proposed in this paper is feasible, which is superior to MFL testing and other electromagnetic methods in many aspects. This method has expended the application range of eddy current non-destructive testing and provided guidance for the quantitative evaluation of pipeline cracks.

ACKNOWLEDGMENT

This work was supported by the National Natural Science Foundation of China (Grant numbers 51575331, 51175316 and 61603238) and Jiangsu Province University Outstanding Science and Technology Innovation Team Project (2019SJK07).

REFERENCES

[1] R. Grimberg, "Electromagnetic nondestructive evaluation: Present and future," *Strojniški vestnik – Journal of Mechanical Engineering*, vol. 2011, no. 3, pp. 204-217, Mar. 2011.

[2] K. Miya, "Recent advancement of electromagnetic nondestructive inspection technology in Japan," *IEEE Transactions on Magnetics*, vol. 38, no. 2, pp. 321-326, Apr. 2002.

[3] A. Sophian, G. Y. Tian, D. Taylor, and J. Rudlin, "Electromagnetic and eddy current NDT: A review," *Insight - Non-Destructive Testing and Condition Monitoring*, vol. 43, no. 5, pp. 302-306, May 2001.

[4] H. A. Sabbagh, R. K. Murphy, E. H. Sabbagh, J. C. Aldrin, J. Knopp, and M. Blodgett, "Computational electromagnetics and model-based inversion: A modern paradigm for eddy-current nondestructive evaluation," *Applied Computational Electromagnetics Society Journal*, vol. 24, no. 6, pp. 533-540, Dec. 2009.

[5] J. García-Martín, J. Gómez-Gil, and E. Vázquez-Sánchez, "Non-destructive techniques based on eddy current testing," *Sensors*, vol. 11, no. 3, pp. 2525-2565, Feb. 2011.

[6] D. Rifai, A. N. Abdalla, K. Ali, and R. Razali, "Giant magnetoresistance sensors: A review on structures and non-destructive eddy current testing applications," *Sensors*, vol. 16, no. 3, pp. 1-30, Mar. 2016.

[7] Y. Li, J. Wilson, and G. Y. Tian, "Experiment and simulation study of 3D magnetic field sensing for magnetic flux leakage defect characterisation," *NDT & E International*, vol. 40, no. 2, pp. 179-184, Mar. 2007.

[8] M. Ravan, R. K. Amineh, S. Koziel, N. K. Nikolova, and J. P. Reilly, "Sizing of 3-D arbitrary defects using magnetic flux leakage measurements," *IEEE Transactions on Magnetics*, vol. 46, no. 4, pp. 1024-1033, May 2010.

[9] J. J. Chen, "3-D defect profile reconstruction from magnetic flux leakage signals in pipeline inspection using a hybrid inversion method," *Applied Computational Electromagnetics Society Journal*, vol. 32, no. 9, pp. 826-832, Sep. 2017.

[10] C. K. Low and B. S. Wong, "Defect evaluation using the alternating current field measurement technique," *Insight - Non-Destructive Testing and Condition Monitoring*, vol. 46, no. 10, pp. 598-605, Oct. 2004.

[11] J. H. Ge, W. Li, G. M. Chen, and X. K. Yin, "Analysis of signals for inclined crack detection through alternating current field measurement with a U-shaped probe," *Insight - Non-Destructive Testing and Condition Monitoring*, vol. 59, no. 3, pp. 121-128, Mar. 2017.

[12] X. C. Hu, "Pulsed alternating current field measurement technique for defect identification and quantification," *Journal of Mechanical Engineering*, vol. 47, no. 4, pp. 121-128, Jan. 2011.

[13] F. Jiang, S. L. Liu, S. J. Xin, and H. L. Zhang, "Electromagnetic nondestructive testing model and surface magnetic field analysis for circumferential cracks on metal rod," *ASME - Journal of Non-destructive Evaluation, Diagnostics and Prognostics of Engineering Systems*, vol. 2, no. 4, pp. 044501, Nov. 2019.

[14] T. Theodoulidis and J. R. Bowler, "Eddy-current interaction of a long coil with a slot in a conductive plate," *IEEE Transactions on Magnetics*, vol. 41, no. 4, pp. 1238-1247, Apr. 2005.

[15] F. Jiang, S. L. Liu, S. J. Xin, et al., "Evaluation of circumferential cracks in metal tube based on magnetic field response model of eddy current testing," *Insight - Non-Destructive Testing and Condition Monitoring*, vol. 62, no. 2, pp. 91-97, Feb. 2020.

[16] Z. Zeng, L. Udpa, and S. S. Udpa, "Finite-element model for simulation of ferrite-core eddy-current probe," *IEEE Transactions on Magnetics*, vol. 46, no. 3, pp. 905-909, Apr. 2010.

[17] Y. Wei and S. L. Liu, "Numerical analysis of the dynamic behavior of a rotor-bearing-brush seal system with bristle interference," *Journal of*

Mechanical Science and Technology, vol. 33, no. 8, pp. 1-9, Aug. 2019.

[18] B. Helifa, M. Féliachi, I. K. Lefkaier, and B. Fouad, "Characterization of surface cracks using eddy current NDT simulation by 3D-FEM and inversion by neural network," *Applied Computational Electromagnetics Society Journal*, vol. 31, no. 2, pp. 187-194, Feb. 2016.

Feng Jiang was born in Yancheng, China, in 1981. He received the M.Sc. degree in the School of Mechanical Engineering from Jiangsu University, Zhenjiang, China, in 2006 and received Ph.D. degree from Shanghai University, Shanghai, China, in 2019. He is currently working as an Associate Professor in Electrical and Information Engineering at Changzhou Institute of Technology. His research interests include electromagnetic nondestructive evaluation, mathematical modeling and fault diagnosis.

Shulin Liu was born in 1963 and received the M.Sc. degree in the School of Mechanical Engineering from Yanshan University, Qinhuangdao, China, in 1989 and received his Ph.D. degree from Harbin Institute of Technology, Harbin, China, in 2003. Since 2008, he is a Professor and Doctoral Supervisor at School of Mechatronics Engineering and Automation, Shanghai University, China. His major research direction is complex equipment fault diagnosis.